Nanoscale

Accepted Manuscript

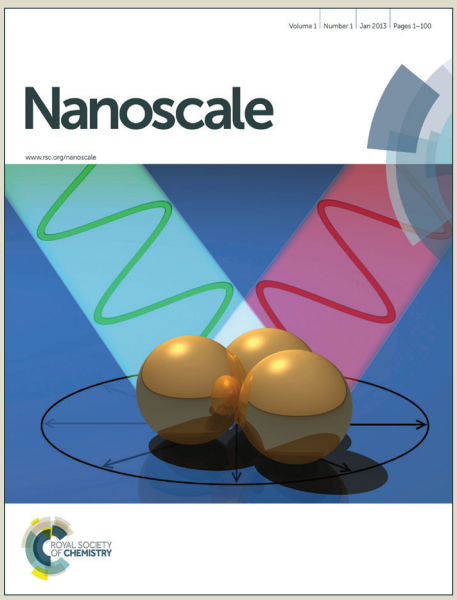

ROYAL SOCIETY OF CHEMISTRY

www.rsc.org/nanoscale

Nanoscale

RSCPublishing

ARTICLE

Guest-host interactions and their impacts on structure and performance of nano-MoS_2

Cite this: DOI: 10.1039/x0xx00000x

Xuefeng Wang, Zhaoruxin Guan, Yejing Li, Zhaoxiang Wang* and Liquan Chen

Received 00th January 2012,
Accepted 00th January 2012

DOI: 10.1039/x0xx00000x

www.rsc.org/

Different guest species, including amorphous carbon, polyvinyl pyrrolidone (PVP), ethylene diaminetrimolybdate (EDA) derived small molecules, have been successfully intercalated into nano-scaled MoS_2 (nano-MoS_2). They bridge the MoS_2 slabs through chemical bonding and their host-guest interactions influence the structure and electrochemical performances of nano-MoS_2. When applied in lithium (Li) and sodium (Na) ion batteries, these MoS_2 nanostructures exhibit distinguished intercalation thermodynamics and cycling performances. These findings shed light on the design of MoS_2 nanostructures and other two-dimensional layer-structured materials.

Introduction

Two-dimensional (2D) layered metal dichalcogenides consist of three interconnected, hexagonally coordinated atomic sulfur-metal-sulfur (S-M-S) sheets[1, 2]. The weak van der Waals force between the S-M-S slabs permits the entrance of some guest species therein. The properties of these intercalation compounds are closely related to the host-guest interactions as well as the chemical properties of the guest atoms or molecules[3, 4]. The intercalation compounds and their intercalation chemistry are the basic science and technology for various technical applications[5-8].

Molybdenum disulfide MoS_2, a typical metal dichalcogenides, has been widely applied in catalysis[9, 10], sensing[11-15], electronic and optical devices[16-18] and electrochemical cells[19, 20]. Introduction of guest species into MoS_2 can change its structure and properties significantly. For example, intercalation of promoter elements, such as Ni and Co, can enhance the catalytic activity of MoS_2 for hydrodesulfuration [21]. Depending on the state of confinement, MoS_2 can be photochemically active over a wide range of wavelength, thus promising for efficient light harvesting[22]. A better understanding of this host-guest interaction is essential for material design and applications.

As a promising anode material for lithium- (Li) and sodium- (Na) ion batteries[20, 23-25], MoS_2 has a theoretical Li or Na storage capacity of 670 mAh g^{-1}. Nano-scaled treatment further improves its rate performance[26-28]. However, less attention was paid to the impact of guest molecules or atoms on the electrochemical performances of MoS_2 in the previous studies. It is interesting to explore how the pre-intercalated guest species interact with the host and what influence these interactions will bring on the Li or Na ion intercalation performance of MoS_2.

Herein, various atoms or molecules are embedded in nano-MoS_2 and their impacts on the physical properties and electrochemical properties of nano-MoS_2 are characterized. When applied as electrode materials for Li- and Na-ion batteries, these nano-MoS_2 intercalation compounds show improved electrochemical performances. Therefore, pre-intercalation of some guest species can be an effective method to modify the electrochemical properties of the nano-MoS_2 electrode materials.

Results and discussion

Nano-MoS_2 with various guest species was prepared by hydrothermally treating different precursors and additives. The obtained products with no additives, and those with glucose, polyvinyl pyrrolidone (PVP), ethylenediaminetrimolybdate (EDA) as the additive, were denoted as GMS, GMS-C, MoS_2-PVP and MoS_2-EDA, respectively.

Figure 1 compares the XRD patterns of commercial MoS_2 and the nano-MoS_2 containing various intercalated guest species. It seems that intercalation of the guest species does not change the symmetry of the lattice. The broadening of the diffraction peaks is attributed to the lowered crystallinity of nano-MoS_2. Intercalation of the guest species pushes the (002) diffraction peak of the nano-MoS_2 to lower angles, indicating an expansion of their cells along the *c* axis. The *c* value of the nano-MoS_2 is calculated to be 6.63, 7.05, 10.02, 11.59 Å, for GMS, MoS_2-PVP, MoS_2-EDA, and GMS-C, respectively. The drastic shift of the (110) peak for MoS_2-PVP and MoS_2-EDA is ascribed to the enlarged *a* value of MoS_2 though no diffraction peaks related to PVP and EDA are found in these two samples. In

addition, the appearance of (004) peak (*ca.* 17.6°) of MoS_2-EDA may be ascribed to the few layers of nanosheets.

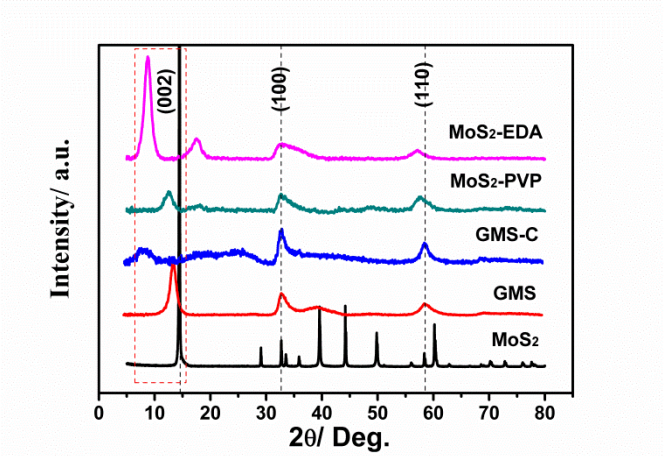

Figure 1. the XRD patterns of various MoS_2

The morphology of the nano-MoS_2 is highly dependent on the additive used (Figure 2). The particles of commercial MoS_2 are a few microns large with small fragments on the surface (Figure 2a). Both GMS and GMS-C are microspheres composed of graphene-like sheets (Figure 2b and Figure 2c). Addition of PVP as a surfactant yields well-dispersed nanospheres of about 100 nm in size (Figure 2d). Through an anion-exchange reaction of the hybrid inorganic-organic MoO_3-EDA nanowires[29, 30], flower-like MoS_2-EDA tubes and microspheres composed of nanosheets (Figure 2e and Figure 2f) are obtained. These nanostructures are beneficial for improving the Li and Na storage performance of MoS_2, due to its increased surface area and shortened diffusion lengths.

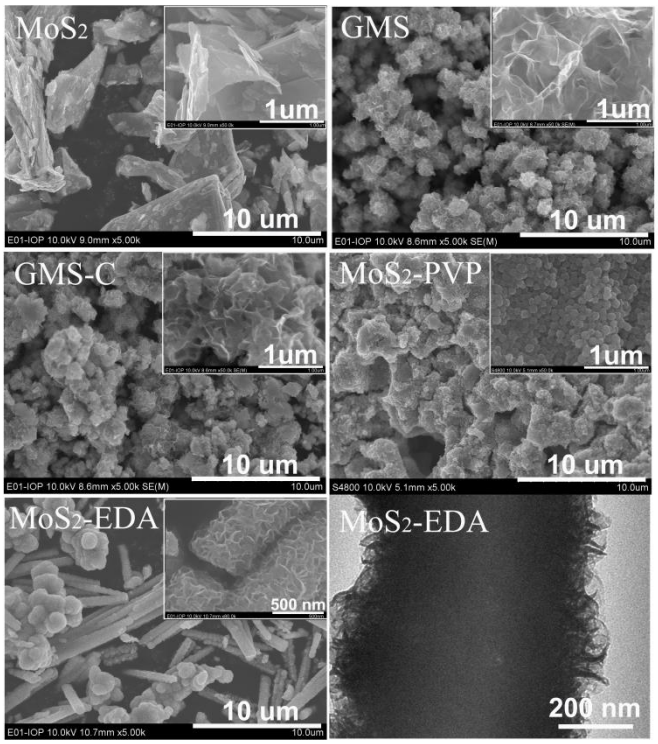

Figure 2. SEM images of commercial MoS_2 (a) and various nano-MoS_2 (b to e, and their insets) and the TEM images (f) of MoS_2-EDA.

In order to distinguish the intercalated species and clarify the host-guest interaction, Fourier-transformed infrared (FTIR), Raman scattering and X-ray photoelectron spectroscopy (XPS) are combined to characterize the structure of MoS_2. As shown in Figure 3a, the embedded organic molecules are decomposed amorphous carbon in GMS-C after annealed at 800°C, showing apparent bands at 1629, 1221, and 1061 cm^{-1} for the residual C=O and C-O groups, respectively. The presence of some PVP characteristic bands and the shifting of the C=O band (from 1673 cm^{-1} in pure PVP to 1650 cm^{-1} in MoS_2-PVP) imply that PVP molecules have been intercalated into MoS_2 and interact with the host MoS_2. Hydrothermal treatment of MoS_2 in EDA embeds some small molecules containing C-N (1583 cm^{-1}) and C=O groups in MoS_2. These molecules bridge the MoS_2 slabs through the S=O (1034 cm^{-1}), C-O-S (949-831 cm^{-1}) and C-S (594 cm^{-1}) bonds.

The S-Mo-S stretching within the basal plane Raman active E_{2g} mode (383 cm^{-1})[31] becomes weak in the nano-MoS_2 (Figure 3b) due to the expansion of the interlayer space. The enhancement of the E_{1g} mode (286 cm^{-1}) [31] and attenuation of A_{1g} mode (408 cm^{-1}) [31] demonstrate that the S atoms are more active in the basal plane than along the *c* axis, especially for MoS_2-EDA. Furthermore, the second order Raman modes, such as $2A_{1g}$ (416 cm^{-1}) [32], become significant in nano-MoS_2. In addition, a new band at 330 cm^{-1} and its second order mode at 660 cm^{-1} appear in nano-MoS_2. These two bands are referred to the Mo-S-O vibrations[33, 34]. Therefore, combination of the FTIR and Raman spectroscopy suggests that amorphous carbon, EDA-derived small molecules and PVP bridge the MoS_2

interlayers through C-S, O-S bonding for GMS-C, MoS_2-EDA and MoS_2-PVP.

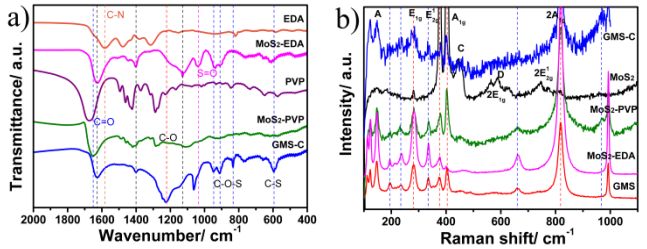

Figure 3. The FTIR (a) and Raman (b) spectra of various nano-MoS_2 samples

Intercalation of these guest species results in red-shifting of the Mo 3d, Mo 2p and S 2p binding energies, 1.7 and 1.1 eV for MoS_2-PVP and MoS_2-EDA, respectively (Figure 4a and Figure 4b), demonstrating the strong host-guest interactions. The guest-free GMS shows the same Mo 3d and S 2p binding energies as those of commercial MoS_2, but the active S atoms of nano-MoS_2 tend to react with oxygen to form SO_4^{2-} (169.2 eV)[35], for example. In contrast, lower-valence oxides are formed in GMS-C, MoS_2-PVP and MoS_2-EDA (Figure 4b). In addition, the XPS spectra confirm the presence of the intercalated species in nano-MoS_2. As shown in Figure 4c and Figure 4d, the obvious C-N (287.7 eV; Figure 4c)[36] , N-C=O (399.7 eV; Figure 4d)[36] and N-H (401.7 eV; Figure 4d) bands in MoS_2-PVP are related to the intercalated PVP. The N-C=O and N-H (Figure 4d) in MoS_2-EDA belong to some EDA-derived small molecules.

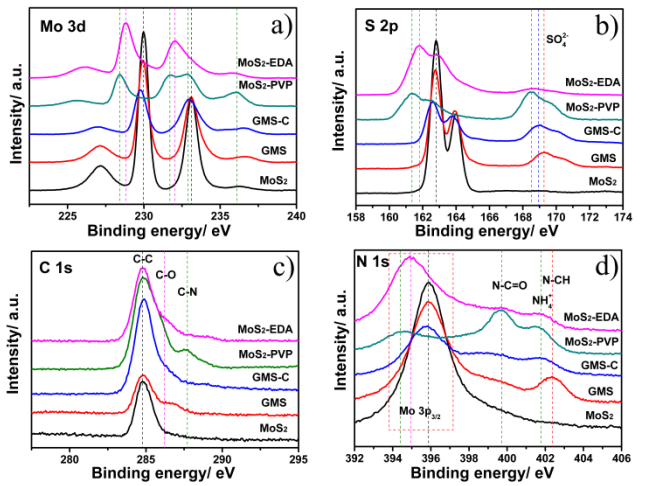

Figure 4. XPS spectra of different MoS_2

Thermogravimetric (TG) and differential scanning calorimetry (DSC) are combined to evaluate the structural stability of nano-MoS_2 and determine the content of MoS_2 phase (Figure 5a and Figure 5b). Based on the setup point of oxidation process, the content of the MoS_2 phase in GMS, GMS-C, MoS_2-PVP and MoS_2-EDA is figured out to be 91, 79, 87, 83 wt%, respectively (Figure 5a). With higher chemical activity, nano-MoS_2 tends to be oxidized at a lower temperature than commercial MoS_2; the main exothermic peak of GMS appears at 327 °C while that of commercial MoS_2 appears at 517 °C. However, the oxidation temperature of the nano-MoS_2 becomes higher after intercalation of the guest species, in the order of MoS_2-EDA > MoS_2-PVP > GMS-C > GMS (Figure 5b). This rank happens to agree with the ranking of the XPS results (Figure 4b; lower-valence sulfur oxides). Therefore, intercalation of some molecules helps to improve the structural stability of nano-MoS_2 due to the chemical bonding (C-S and O-S bonding) between the intercalated molecules and MoS_2 slabs.

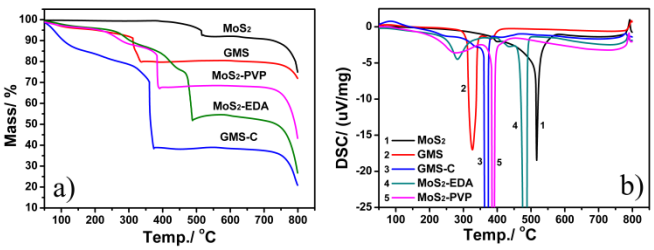

Figure 5. The TG (a) and DSC traces (b) of various nano-MoS_2 samples

The above results make a comprehensive understanding of various MoS_2 nanostructures. The nano-MoS_2 samples, GMS for example, show high chemical activity and low structural stability. On the other hand, the intercalated molecules bridge the MoS_2 slabs by the C-S, O-S bonding, decreasing the activity of the S atoms in the slabs and enhancing the structural stability of the nano-MoS_2. These host-guest interactions have important impact on the electrochemical performances of MoS_2.

MoS_2 has been studied as a promising anode material in terms of charge capacity, rate capability and cycle life for Li-ion batteries[20] and for Na-ion batteries[23-25]. Our previous work[19, 37] indicated that Li and Na has similar intercalation mechanisms in MoS_2. The guest-host interactions affect the intercalation thermodynamics of the nano-MoS_2, leading to different potential profiles, especially for the MoS_2-PVP sample (Figure 6). Only one plateau appears at low potential in the Li (Na) intercalation potential profile of MoS_2-PVP but several plateaus or slopes exist in that of the other MoS_2 nanostructures. This is supposed to be due to the presence of chemically reduced $[MoS_2]^-$ in MoS_2-PVP as is evidenced with the low valence of Mo and S atoms (1.7 eV red-shifting in above XPS spectra) as well as the polarization caused by the existence of PVP molecules.

As shown in Figure 6c and Figure 6d, GMS-C and MoS_2-PVP exhibit superior cycling stability and their capacities increase with cycling. In terms of capacity and cycling stability, MoS_2-EDA shows the best electrochemical performance. A high reversible Na-storage capacity of 565 mAh g^{-1} is obtained for MoS_2-EDA, higher than any of the reported values[23-25, 38]. This outstanding electrochemical performance is ascribed to the presence of guest species. The C-S and O-S bonding enhances the structural stability of the nano-MoS_2. Even when MoS_2 is decomposed into Mo and Li_2S upon full Li or Na insertion, these interactions still take effect in anchoring the polysulfides

and, therefore, enhancing the cycling stability of the nano-MoS_2 [39].

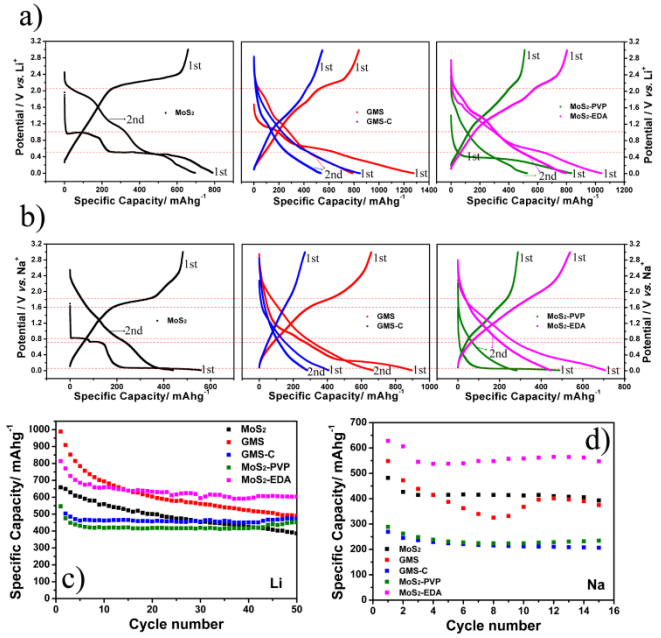

Figure 6. Comparison of the potential profiles (a, b), and cycle performance (c, d) of various (nano-)MoS_2 (a, c for Li-ion batteries and b, d for Na-ion batteries)

Conclusions

Nano-MoS_2 materials with various embedded guest species are compared to explore the impacts of host-guest interaction on its physical and electrochemical properties. The embedded PVP and EDA-derived small molecules bridge the interlayer of MoS_2 through C-S, O-S bonding. Drastic influences of MoS_2 are observed on its structure and structural stability. In addition, the host-guest interaction alters the intercalation thermodynamics and cycling stability of nano-MoS_2 as anode material for Li- and Na-ion batteries. These findings will shed light on the future material design and applications of nano-MoS_2.

Acknowledgements

This work was financially supported by the National Natural Science Foundation of China (NSFC No. 51372268) and the National 973 Program of China (2009CB220100).

Notes and references

[a] Key Laboratory for Renewable Energy, Chinese Academy of Sciences Beijing Key Laboratory for New Energy Materials and Devices, Beijing National Laboratory for Condensed Matter Physics, Institute of Physics, Chinese Academy of Sciences, P.O. Box 603, Beijing 100190, China
Email: zxwang@iphy.ac.cn

Electronic Supplementary Information (ESI) available: Experimental section. See DOI: 10.1039/b000000x/

1. M. Chhowalla, H. S. Shin, G. Eda, L.-J. Li, K. P. Loh and H. Zhang, *Nat Chem*, 2013, **5**, 263-275.
2. X. Huang, Z. Zeng and H. Zhang, *Chem. Soc. Rev.*, 2013, **42**, 1934-1946.
3. A. D. Yoffe, *Solid State Ionics*, 1990, **39**, 1-7.
4. E. Benavente, M. A. Santa Ana, F. Mendizábal and G. González, *Coord. Chem. Rev.*, 2002, **224**, 87-109.
5. V. Etacheri, R. Marom, R. Elazari, G. Salitra and D. Aurbach, *Energy Environ. Sci.*, 2011, **4**, 3243-3262.
6. J. B. Goodenough and Y. Kim, *Chem. Mater.*, 2009, **22**, 587-603.
7. M.-R. Gao, Y.-F. Xu, J. Jiang and S.-H. Yu, *Chem. Soc. Rev.*, 2013, **42**, 2986-3017.
8. Z. Zeng, Z. Yin, X. Huang, H. Li, Q. He, G. Lu, F. Boey and H. Zhang, *Angew. Chem. Int. Ed.*, 2011, **50**, 11093-11097.
9. M. A. Albiter, R. Huirache-Acuna, F. Paraguay-Delgado, J. L. Rico and G. Alonso-Nunez, *Nanotechnology*, 2006, **17**, 3473-3481.
10. X. Huang, Z. Zeng, S. Bao, M. Wang, X. Qi, Z. Fan and H. Zhang, *Nat Commun*, 2013, **4**, 1444.
11. Q. H. Wang, K. Kalantar-Zadeh, A. Kis, J. N. Coleman and M. S. Strano, *Nat Nano*, 2012, **7**, 699-712.
12. C. Zhu, Z. Zeng, H. Li, F. Li, C. Fan and H. Zhang, *J. Am. Chem. Soc.*, 2013, **135**, 5998-6001.
13. Q. He, Z. Zeng, Z. Yin, H. Li, S. Wu, X. Huang and H. Zhang, *Small*, 2012, **8**, 2994-2999.
14. S. Wu, Z. Zeng, Q. He, Z. Wang, S. J. Wang, Y. Du, Z. Yin, X. Sun, W. Chen and H. Zhang, *Small*, 2012, **8**, 2264-2270.
15. H. Li, Z. Yin, Q. He, H. Li, X. Huang, G. Lu, D. W. H. Fam, A. I. Y. Tok, Q. Zhang and H. Zhang, *Small*, 2012, **8**, 63-67.
16. S. Balendhran, S. Walia, H. Nili, J. Z. Ou, S. Zhuiykov, R. B. Kaner, S. Sriram, M. Bhaskaran and K. Kalantar-zadeh, *Adv. Funct. Mater.*, 2013, **23**, 3952-3970.
17. Z. Yin, H. Li, H. Li, L. Jiang, Y. Shi, Y. Sun, G. Lu, Q. Zhang, X. Chen and H. Zhang, *ACS Nano*, 2011, **6**, 74-80.
18. J. Liu, Z. Zeng, X. Cao, G. Lu, L.-H. Wang, Q.-L. Fan, W. Huang and H. Zhang, *Small*, 2012, **8**, 3517-3522.
19. X. P. Fang, C. X. Hua, X. W. Guo, Y. S. Hu, Z. X. Wang, X. P. Gao, F. Wu, J. Z. Wang and L. Q. Chen, *Electrochim. Acta*, 2012, **81**, 155-160.
20. T. Stephenson, Z. Li, B. Olsen and D. Mitlin, *Energy Environ. Sci.*, 2014, **7**, 209.
21. L. S. Byskov, J. K. Nørskov, B. S. Clausen and H. Topsøe, *J. Catal.*, 1999, **187**, 109-122.
22. P. Pramanik and S. Bhattacharya, *Mater. Res. Bull.*, 1990, **25**, 15-23.
23. L. David, R. Bhandavat and G. Singh, *ACS Nano*, 2014, **8**, 1759-1770.
24. J. Park, J.-S. Kim, J.-W. Park, T.-H. Nam, K.-W. Kim, J.-H. Ahn, G. Wang and H.-J. Ahn, *Electrochim. Acta*, 2013, **92**, 427-432.
25. C. Zhu, X. Mu, P. A. van Aken, Y. Yu and J. Maier, *Angew Chem Int Ed Engl*, 2014, **53**, 2152-2156.
26. J.-Z. Wang, L. Lu, M. Lotya, J. N. Coleman, S.-L. Chou, H.-K. Liu, A. I. Minett and J. Chen, *Advanced Energy Materials*, 2013, **3**, 798-805.
27. J. Xiao, D. Choi, L. Cosimbescu, P. Koech, J. Liu and J. P. Lemmon, *Chem. Mater.*, 2010, **22**, 4522-4524.
28. C. Wang, W. Wan, Y. Huang, J.-T. Chen, H. Zhou and X. Zhang, *Nanoscale*, 2014, **6**, 5351-5358.
29. S. Zhuo, Y. Xu, W. Zhao, J. Zhang and B. Zhang, *Angew Chem Int Ed Engl*, 2013, **52**, 8602-8606.
30. Q. Gao, S. Wang, H. Fang, J. Weng, Y. Zhang, J. Mao and Y. Tang, *J. Mater. Chem.*, 2012, **22**, 4709-4715.
31. T. J. Wieting and J. L. Verble, *Physical Review B*, 1971, **3**, 4286-4292.
32. J. M. Chen and C. S. Wang, *Solid State Commun.*, 1974, **14**, 857-860.
33. X. L. Li and Y. D. Li, *J. Phys. Chem. B.*, 2004, **108**, 13893-13900.
34. A. Loewenschuss, J. Shamir and M. Ardon, *Inorg. Chem.*, 1976, **15**, 238-241.
35. A. G. Schaufuß, H. W. Nesbitt, I. Kartio, K. Laajalehto, G. M. Bancroft and R. Szargan, *J. Electron Spectrosc. Relat. Phenom.*, 1998, **96**, 69-82.
36. Y. Mao, H. Duan, B. Xu, L. Zhang, Y. Hu, C. Zhao, Z. Wang, L. Chen and Y. Yang, *Energy Environ. Sci.*, 2012, **5**, 7950-7955.
37. X. Wang, X. Shen, Z. Wang, R. Yu and L. Chen, 2014.
38. G. S. Bang, K. W. Nam, J. Y. Kim, J. Shin, J. W. Choi and S.-Y. Choi, *ACS Applied Materials & Interfaces*, 2014, **6**, 7084-7089.

39. Z. W. Seh, Q. Zhang, W. Li, G. Zheng, H. Yao and Y. Cui, *Chemical Science*, 2013, **4**, 3673-3677.